

Numerical counterparts of GRB host galaxies

S. Courty^{1,2}, G. Björnsson & E. H. Gudmundsson

¹*Science Institute, University of Iceland, Dunhaga 3, IS-107 Reykjavik, Iceland*

²*Laboratoire de l'Univers et de ses Théories, CNRS UMR 8102,*

Observatoire de Paris-Meudon, 5 place Jules Janssen, 92195 Meudon, France

e-mail: courty, gulli, einar@raunvis.hi.is

11 June 2021

ABSTRACT

We explore galaxy properties in general and properties of host galaxies of gamma-ray bursts (GRBs) in particular, using N-body/Eulerian hydrodynamic simulations and the stellar population synthesis model, *Starburst99*, to infer observable properties. We identify simulated galaxies that have optical star formation rate (SFR) and SFR-to-luminosity ratio similar to those observed in a well-defined sample of ten host galaxies. Each of the numerical counterparts are found in catalogs at the same redshifts as the observed hosts. The counterparts are found to be low-mass galaxies, with low mass-to-light ratio, recent epoch of formation, and high ratio between the SFR and the average of the SFR. When compared to the overall galaxy population, they have colors much bluer than the high-mass star-forming galaxy population. Although their SFRs span a range of values, the specific rates of the numerical counterparts are equal to or higher than the median values estimated at the different redshifts. We also emphasize the strong relationships between the specific star formation rate (SFR) and quantities known to reflect the star formation history of galaxies, i.e. color and mass-to-light ratio: At intermediate redshift, the faintest and bluest galaxies are also the objects with the highest specific rates. These results suggest that GRB host galaxies are likely to be drawn from the high specific SFR sub-population of galaxies, rather than the high SFR galaxy population. Finally, as indicated by our catalogs, in an extended sample, the majority of GRB host galaxies is expected to have specific SFRs higher than found in the magnitude-limited sample studied here.

Key words: cosmology: large-scale structure of Universe – galaxies: formation – galaxies: evolution – gamma rays: bursts

1 INTRODUCTION

Galaxies with a wide variety of properties are observed in the universe and galaxy sub-populations contribute in a different way to the overall galaxy properties at different redshifts. Important questions in present day cosmology include investigations into how the different sub-populations can be characterized, how sub-populations formed at high redshift evolve into galaxies in the local universe and how these populations contribute to various properties of the overall galaxy population. In this paper we use a numerical approach to extend our investigation of galaxy properties (Courty et al. 2004, hereafter referred to as Paper I) that focused on the specific star formation rate. While the star formation rate is a ‘snapshot’ of the stellar activity in a galaxy, the specific rate is an indicator of how the galaxy forms its stellar mass relative to the total mass that has been assembled through its entire lifetime, via mergers and/or transformation of new accreted gas. The specific rate

should therefore give some insight into the star formation history of galaxies, as do other properties, such as colors. The specific SFR has been estimated in a number of observational studies: Guzman et al. (1997) compare the specific SFRs of compact blue galaxies with other galaxy populations, Brinchmann et al. (2004) discuss the star-forming galaxies of the SDSS, Bell et al. (2005) combine infrared data from the *Spitzer Space Telescope* with optical data, and Feulner et al. (2005) estimate the specific SFR up to $z = 5$.

As in Paper I, we here focus on the properties of a particular population of galaxies, namely the host galaxies of long-duration gamma-ray bursts. The nature of the hosts and their evolution with redshift are still open questions. The emphasis over the last few years has been on the host galaxies of long-duration GRBs, which are seen as a powerful tracer of massive star formation in the universe. It is now well established that at least some long-

arXiv:astro-ph/0701762v1 26 Jan 2007

duration GRBs occur at the death of massive stars (e.g. Hjorth et al. 2003; Stanek et al. 2003) and in a cosmological context massive stars are very short-lived. Because of their extreme brightness, long-duration GRBs are an effective way of locating distant galaxies, most of which are so faint that they would go undetected in galaxy surveys. In fact, host galaxies fainter than magnitude 29 have already been detected (Jaunsen et al. 2003). In addition, GRBs have been detected out to a redshift higher than $z = 6$, and will likely be detected to even higher redshifts. Rather detailed studies of the local star forming regions in the hosts is therefore possible (Berger et al. (2005), Berger et al. (2005)). The most distant burst to date, GRB 050904 at $z = 6.29$ (Tagliaferri et al. 2005; Kawai et al. 2005), has already revealed a number of interesting properties of the interstellar medium of the host (Totani 2005), while information about galaxy formation and evolution is yet to be explored in detail, mostly awaiting the increase of the currently modest sample size (around 50 hosts).

From individual studies of host galaxies of GRBs (Fruchter et al. 1999; Fynbo et al. 2003), comparison of host samples with other sources detected in various deep surveys (Le Floch et al. 2003), and statistical stellar population synthesis of the optical and near-infrared host properties (Sokolov et al. 2001; Chary et al. 2002; Christensen et al. 2004), indications are that host galaxies have particular characteristics: These galaxies tend to be optically sub-luminous, low-mass, blue, star-bursting galaxies, with young stellar populations, a modest activity of optical star formation, and perhaps low-metallicity and modest amount of dust obscuration, although this last feature still needs to be firmly established. Le Floch et al. (2003) compare a large sample of host galaxies of GRBs, observed in the near infrared, with various galaxy surveys and find that the observed K and R -band magnitudes of the hosts are comparable to the field sources selected in optical/N-IR deep surveys, but differ significantly from luminous and dusty starburst galaxies observed with ISO and SCUBA. Moreover they show blue $R - K$ colors typical of the faint blue galaxy population in the field at $z = 1$. Also, SCUBA sub-millimeter observations of GRB host galaxies performed by Smith et al. (2005) suggest that most hosts are not luminous dusty star-forming galaxies. Furthermore, Christensen et al. (2004) have studied a magnitude-limited sample of hosts and estimate the ratio between the rest-frame UV star formation rate and the host optical luminosity. They suggest that the hosts are similar to those HDF galaxies that have the highest SFR-to-luminosity ratios.

In Paper I, we showed that among the population still actively forming stars at low redshift, the high-mass galaxies have much lower specific SFR than the low-mass galaxies. The non star-forming galaxies, that span the whole galaxy mass range, are old galaxies while most of the stellar populations in the high specific SFR galaxies formed recently. At high redshift the trend of increasing specific SFR with decreasing galaxy mass is also seen, but an interesting point is that the cosmological evolution is much stronger for the high-mass than the low-mass galaxies. These trends agree in general well with the aforementioned observational estimates, to the extent that we concentrate on the qualitative behavior of the specific SFR. Although not based on observable properties, the results of Paper I for the specific

SFR suggest that a sub-population of faint and blue galaxies, some of the characteristics of the GRB hosts, are likely to belong to the high specific SFR galaxy population, rather than the high-SFR population.

In this paper, we extend the discussion of the properties of GRB host galaxies in Paper I, by combining the results of the same simulations as in that paper with the stellar population synthesis (SPS) code, *Starburst99* (Vázquez et al. 2005), to infer observable properties. SPS codes allow us to compute the spectral energy distributions of the simulated galaxies at different redshifts. We identify simulated galaxies that have both similar rest-frame ultraviolet SFRs and ratios between this SFR and the B -band luminosity as the ten observed hosts of a well-defined sample (Christensen et al. (2004), hereafter Chr04). The numerical counterparts of these observed hosts are characterized by a variety of properties, estimated either directly from the simulation or from the computation of the SEDs. In particular, for each galaxy we determine the mass, the ratio between the SFR and the average of the SFR, $SFR^*/\langle SFR \rangle$, the specific SFR, the epoch of formation, the $R - K$ color, and the mass-to-light ratio. The properties of the counterparts are then compared to the overall galaxy population, that is characterized through the close relationships between the specific SFR and the color index and mass-to-light ratio. This comparison is, however, limited by the fact that the observed sample still only includes 10 hosts, spanning a large redshift range.

Although fairly small, the sample of Chr04 is the only available homogeneous sample that estimates the ratio between the optical SFR and the luminosity. Information on other hosts does exist in the literature and other studies, e.g. Sollerman et al. (2005), use different star formation rate estimators such as $SFR_{H\alpha}$ and SFR_{OII} , rather than the UV-based indicator adopted in Chr04, but only for a couple of hosts. A comprehensive study of a large host sample using all available information awaits future studies. In Section 3 we also briefly discuss the counterparts of GRB 000911 and 030329, whose SFR_{UV} and M_B values are available in Masetti et al. (2005) and Gorosabel et al. (2005), respectively.

The paper is organized as follows: In Section 2, we describe briefly the simulation and use of the SPS code. Section 3 contains the main results of the paper. It starts by discussing the observed host sample we use (section 3.1) and the procedure used to identify the numerical counterparts (section 3.2). We discuss the observational properties of the counterparts in section 3.3 and compare their properties with those of the galaxy population in section 3.4. Section 4 concludes the paper.

2 NUMERICAL PROCEDURE

We repeat the simulation used in Paper I in order to obtain galaxy catalogs at the same redshifts as that of the observed GRB hosts in the sample of Chr04. We briefly recall the numerical method and we refer to Paper I for details regarding the simulation. The three dimensional N-body/hydrodynamical code couples a PM scheme for computing gravitational forces with an Eulerian approach for solving the hydrodynamical equations. The dom-

inant processes relevant for galaxy formation are included: Gravitation, hydrodynamical shocks and radiative cooling processes. Collisional ionization equilibrium is not assumed and the cooling rates are explicitly computed from the evolution of a primordial composition hydrogen-helium plasma. The cosmological scenario adopted is a Λ -cold dark matter model with the following parameters: $H_0 = 70 \text{ km s}^{-1} \text{ Mpc}^{-1}$, $\Omega_K = 0$, $\Omega_m = 0.3$, $\Omega_\Lambda = 0.7$, $\Omega_b = 0.02h^{-2}$ with $h = H_0/100$, $\sigma_8 = 0.91$. The comoving size of the computational volume is $32 h^{-1} \text{ Mpc}$ and the simulation has 256^3 dark matter particles and an equal number of grid cells. Galaxy formation is introduced using a phenomenological approach. At each time step, in cells whose gas satisfies given criteria, a fraction of the gas is turned into a stellar particle of mass m_* and epoch of formation a_* , the scale-factor corresponding to the cosmic time, t_* . The criteria are the following: The cooling time must be less than the dynamical time, $t_{\text{cool}} < t_{\text{dyn}}$; the baryonic density contrast, $(1 + \delta_B)$, must be higher than a threshold $(1 + \delta_B)_s = 5.5$; the gas must be in a converging flow, $\nabla \cdot \vec{v} < 0$; and the size of the cell must be less than the Jean's length, given by $\lambda_J = c_s(\pi/G\rho)^{1/2}$. The mass m_* is given by $m_B(t_0)\Delta t/t_*$, where Δt is the timestep, the characteristic time is taken to be $t_* = \max(t_{\text{dyn}}, 10^8 \text{ yr})$, and $m_B(t_0)$ is the baryonic mass enclosed within the grid cell. Galaxy-like objects are then defined, at any redshift, by grouping the stellar particles with a friend-of-friend algorithm. A simulated galaxy is therefore a collection of stellar particles of different masses formed at different epochs.

At any redshift, galaxies are characterized by their mass, M , defined as the sum of the mass of all the stellar particles the galaxy is composed of; an epoch of formation, defined to be the mass-weighted average of the epoch of formation of all its stellar particles; and a star formation rate, SFR^* , defined as the amount of stellar material formed in the previous 10^8 yr . We also estimate the specific star formation rate, $\epsilon \equiv \log(10^{11} \text{ yr } SFR^*/M)$, a quantity that measures the efficiency of the conversion of the gas into stellar material relative to the galaxy mass. We have, as in Paper I, only considered galaxies with a mass higher than $5 \cdot 10^8 M_\odot$ in the simulated catalogs. We refer to Paper I for an illustration of the different sub-populations of galaxies obtained.

Considering each stellar particle as a homogeneous stellar population, the total spectral energy distribution (SED) of a galaxy can be computed from synthesis codes. Evolutionary synthesis codes combine stellar evolutionary theory to describe the time evolution of model stars, stellar atmosphere theory to transform quantities from the theoretical space to the observational one, and the stellar birth rate, giving the number of stars with a given initial mass formed at a given time. The stellar birth rate comes from the star formation history, which gives the number of stars born in a given time, and the initial mass function (IMF), which gives the relative number of stars born as a function of mass (see Cervino & Luridiana (2005) for a discussion regarding the uncertainties of the synthesis codes). In our procedure, the star formation history of a galaxy comes directly from the formation epoch and mass of all its stellar populations as recorded in the simulation. We use the stellar population synthesis model, Starburst99 (Leitherer et al. 1999) in its latest version (Vázquez et al. 2005), to derive observable

properties. The main change in this version is the introduction of the Padova stellar evolutionary tracks, allowing the computation of stellar evolution for old and low-mass stars as well as high-mass stars.

We start by defining a SED template: we consider a single stellar population of $10^6 M_\odot$, assumed to form instantaneously and evolve passively over a maximal time of 15 Gyr. The SED is computed at 1221 points between 91 \AA and $160 \mu\text{m}$. We select in Starburst99 the ‘‘Padova AGB’’ evolutionary tracks, selection of the 1992 – 1994 Padova tracks with thermally pulsing AGB stars added, with a metallicity of $Z = 0.004 = 0.2Z_\odot$, where $Z_\odot \simeq 0.02$. We choose a Salpeter IMF, $dP/dm = m^{-2.35}$, with low and high-mass cut-offs at 0.1 and $100 M_\odot$, respectively. The other input parameters adopted (supernova cut-off mass, black hole cut-off mass, wind model, interpolation in mass method, model atmosphere), are the standard ones. We refer the reader to the Starburst99 website¹ for a full explanation.

The total SED of a galaxy at a given redshift is the sum of the SEDs of all the stellar populations present in the galaxy. The SED of a stellar particle, at a given redshift, is the SED template evolved on the time $t(z) - t_*$, in order to take cosmological expansion into account, and scaled to the mass of the stellar population with the factor $m_*/(10^6 M_\odot)$. To properly include the contribution of those stellar particles that formed at the simulation output time, $t(z)$, the SED is evolved over 10^4 yr . Note that this procedure is applied to the simulated galaxies after the simulation run, and not during it. Nevertheless, the inferred SED of a galaxy accounts for the formation all along the simulation of different stellar populations. A caveat of the procedure is that the simulation does not take into account any evolution of the gas metallicity, and our derived observable properties are based on a single template. Due to the higher UV-luminosities of low-metallicity stars, assuming higher metallicity tracks would decrease the total UV-luminosity. However, in the catalog at $z = 1$ almost all of the non star-forming galaxies have luminosities more than twice the luminosity computed with solar metallicity tracks, whereas there are only 19 star-forming galaxies with such a large luminosity.

Star formation rates can be derived from the UV continuum or the $H\alpha$ luminosity using appropriate proportionality coefficients. These coefficients are derived from stellar population synthesis models, involving an initial mass function (IMF) and star formation history, by looking for a proportionality relation assuming that the star formation rate is constant in the later phases on given timescales. These are roughly 10^7 yr for $H\alpha$ and 10^8 yr for the UV. These coefficients therefore depend on the IMF and its slope, the upper and lower mass cut-off, and the metallicity (Boselli et al. 2001). Since one of the purposes of this paper is to find the numerical counterparts of observed host galaxies, we use the same indicator of the star formation rate as Chr04, and estimate it from the UV continuum at 2800 \AA , although the SFRs of the two hosts at the highest redshifts are estimated using the UV continuum at 1500 \AA in Chr04. The calibration factor used to convert the luminosity at 2800 \AA into SFR is 1.4×10^{-28} , in units of $(M_\odot \text{ yr}^{-1})(\text{erg s}^{-1} \text{ Hz}^{-1})^{-1}$ (Kennicutt 1998). In our procedure the luminosity at 2800

¹ <http://www.stsci.edu/science/starburst99/>

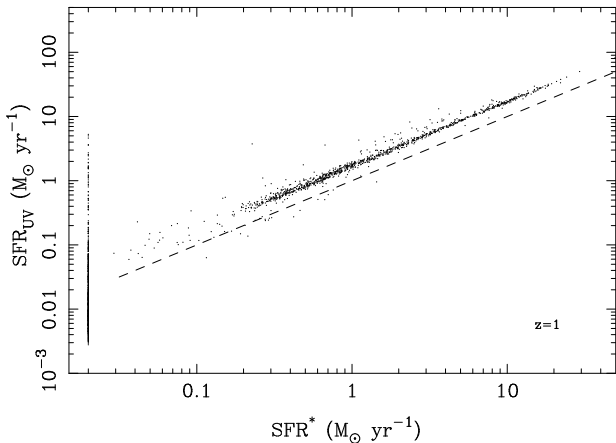


Figure 1. Comparison of the star formation rate SFR^* with SFR_{UV} obtained from the synthetic spectrum for galaxies at $z = 1$. Non-star forming galaxies are for display purposes plotted at $SFR^* = 0.02 M_{\odot} \text{ yr}^{-1}$. The diagonal dashed line shows $SFR_{UV} = SFR^*$.

\AA is obtained by averaging the spectrum over 20 \AA around 2800 \AA . Note that, although our spectral energy distributions are determined at sub-solar metallicity, we adopt the usual calibration to convert the UV luminosity into SFR that is estimated at solar metallicity. At lower metallicity the calibration increases due to the higher luminosity of low-metallicity stars. The SFR of low-metallicity galaxies when estimated with a calibration at solar metallicity is thus overestimated. The evolution of the calibration associated with different SFR indicators is estimated in Sullivan et al. (2001) and Bicker & Fritze-v. Alvensleben (2005), for instance. At $Z = 0.2Z_{\odot}$, the latter paper found that the SFR is overestimated by a factor 1.4, compared to our calibration.

In Figure 1, we compare the SFR^* , computed directly from the simulation, with the SFR estimated from the synthetic spectrum of the simulated galaxies at $z = 1$. Non-star forming galaxies (i.e. with $SFR^*=0$) are for display purposes plotted at $SFR^* = 0.02 M_{\odot} \text{ yr}^{-1}$. At this redshift, the galaxy population includes 1927 objects, with 1148 star-forming galaxies (as expected, the number of non star-forming galaxies is larger at $z = 0$). The diagonal dashed line shows $SFR_{UV} = SFR^*$. Despite the scatter in the diagram, it is clear that the two different estimates are of the same order. The estimate from the simulations is a factor of about 2 lower than that obtained from the synthetic spectra.

Figure 2 shows the B - and K -band magnitudes as functions of the galaxy mass for the simulated catalog at $z = 1$. The B and K -band magnitudes are computed using the “Buser’s $B3$ ” filter and the “IR K filter + Palomar 200 IR detectors + atmosphere 0.57” from the `Galaxev` package (Bruzual & Charlot 2003). Different symbols distinguish star-forming and non star-forming galaxies. Note that both are strongly correlated with the mass. There is much less dispersion in M_K since the B -band luminosities are dominated by the flux from young massive stars whereas L_K is a better tracer of the overall stellar population. The corresponding plots at $z = 0$ would show the same trend although quantitatively different. For instance, the M_K -mass relation shows slightly more dispersion and galaxies at $M_K^* = -24.2$, the

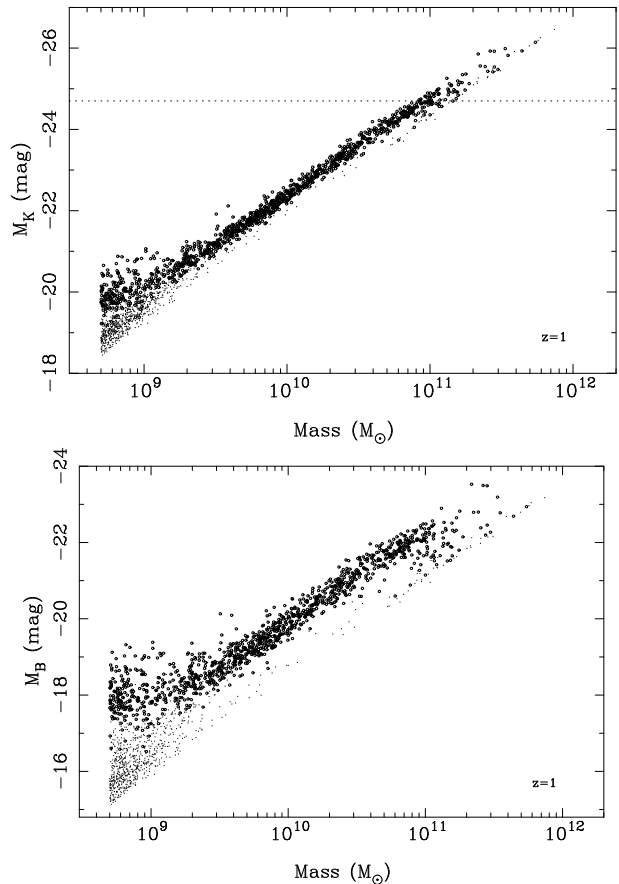


Figure 2. The mass-magnitude diagrams (upper panel: K -band, lower-panel: B -band) for the simulated galaxies at $z = 1$. In both panels, dots denote star-forming galaxies while the small dots denote the non star-forming galaxies. The estimate of $M_{K_s}^* = -24.7$ around $z = 1$ from the K20 galaxy survey (Pozzetti et al. 2003) is marked by the dotted horizontal line.

characteristic magnitude of the galaxy luminosity function in Cole et al. (2001), have a mass of $\sim 10^{11} M_{\odot}$.

In the following sections we consider other quantities to characterize galaxies. The lifetime of a galaxy is estimated at a given redshift, $t(z) - t_{form}$, where t_{form} is the epoch of the formation of the first stellar population. From this the average of the star formation rate, $\langle SFR \rangle$, at a given redshift is determined as the amount of stellar material formed over the lifetime of the galaxy. The SFR^* is compared with the average through the ratio $SFR^*/\langle SFR \rangle$, that may be seen as analogous to the so-called birth-rate parameter, b , (Kennicutt et al. 1994). The mass-to-light ratios in the B and K -bands are estimated using the solar magnitudes of 5.45 and 3.3, respectively, and the color $R - K$ using the “Cousins R” filter from the `Galaxev` package. Finally, the ratio between the rest-frame ultraviolet SFR and the luminosity, $SFR_{UV}/(L_B/L_B^*)$, uses the characteristic magnitude or magnitude at the break of the local galaxy luminosity function, $M_B^* = -21$. This ratio is sometimes called the specific SFR as e.g., in Chr04, but we will refer to it by the term SFR-to-luminosity ratio and reserve the term specific SFR for the ratio between the SFR and the galaxy mass, as is customary in the literature.

Table 1. Properties of the numerical counterparts corresponding to the GRB hosts listed in column one. Following the redshift of the simulated catalog in col. 2, the percentage errors in SFR_{UV} and the SFR-to-luminosity ratio, ΔX and ΔY defined in the text, are given in cols. 3 and 4. Column 5 shows the mass of the counterpart, while col. 6 shows the epoch of its first formed stellar population, t_{form} (see Section 2 for definition) relative to the Hubble time. The mass-to-light ratios in the K and B -bands, respectively, are given in cols. 7 and 8, followed by the corresponding absolute magnitudes. Then comes the color index, $R - K$, and the next to last column lists the $R(AB)$ apparent magnitude. Finally, a reference number for each host is given in the last column.

GRB	z	ΔX	ΔY	$M (M_{\odot})$	$1 - t_{form}/t_H(z)$	M/L_K	M/L_B	M_K	M_B	$R - K$	$R(AB)$	#
000926	2.036	0.7	0.5	1.16×10^{10}	0.76	0.36	0.36	-22.97	-20.83	2.61	24.41	1
990123	1.592	5.6	3.2	2.41×10^{10}	0.81	0.47	0.59	-23.47	-21.08	3.50	24.27	2
000418	1.113	5.6	8.8	8.27×10^9	0.86	0.35	0.32	-22.63	-20.57	2.47	23.24	3
980703	0.963	1.3	0.6	3.68×10^{10}	0.88	0.52	0.66	-23.82	-21.41	2.87	22.18	4
000210	0.843	6.5	5.7	5.16×10^9	0.89	0.47	0.54	-21.79	-19.50	2.61	23.64	5
970508	0.832	3.7	0.3	7.20×10^8	0.89	0.30	0.25	-20.14	-18.18	2.22	24.84	6
991208	0.704	1.2	0.9	1.64×10^9	0.90	0.41	0.45	-20.71	-18.46	2.54	24.24	7
970228	0.695	10.8	0.5	1.60×10^9	0.90	0.49	0.56	-20.49	-18.19	2.51	24.41	8
010921	0.449	1.9	1.1	8.97×10^9	0.92	0.68	1.01	-22.01	-19.42	2.58	21.93	9
990712	0.429	3.3	2.1	1.42×10^9	0.92	0.38	0.36	-20.62	-18.55	2.07	22.71	10

3 THE NUMERICAL COUNTERPARTS OF OBSERVED GRB HOST GALAXIES

In this section we attempt to identify numerical counterparts to the host galaxies of the Ch04 sample, explore their properties, and compare the host candidate population with the overall galaxy population. We first summarize the relevant properties of the observed sample and our approach to identifying the numerical counterparts. We then discuss their observed properties.

3.1 The observed sample

The sample presented in Chr04 is homogeneous and consists of 10 GRB hosts with redshifts between $z = 2.037$ and $z = 0.433$. The sample is magnitude limited ($R < 25.3$) and ensures that hosts are bright enough to make multi-color photometry possible. The first column in Table 1 lists the hosts under consideration. The observationally determined values of SFR_{UV} and $SFR_{UV}/(L_B/L_B^*)$ are given in Table 4 and 5 of Chr04 and we note that the SFR_{UV} entering the SFR-to-luminosity ratio is not corrected for internal extinction, generally found to be moderate or low. The SFR spans a wide range (between 0.8 and $13 M_{\odot} \text{ yr}^{-1}$), but hosts with redshifts higher than 0.9 have the highest SFR_{UV} , more than $\sim 6 M_{\odot} \text{ yr}^{-1}$, whereas hosts at lower redshifts have $SFR_{UV} < 2.5 M_{\odot} \text{ yr}^{-1}$.

Various observational studies of individual hosts of the Chr04 sample result in slightly different estimates of the same properties (Gorosabel et al. (2003) for GRB 000418, Gorosabel et al. (2003) for GRB 000210, Bloom et al. (1999) for GRB 990123, for instance). We have not attempted to collect all the data existing in the literature, and have only considered the SFR_{UV} and $SFR_{UV}/(L_B/L_B^*)$ given in Chr04. All the hosts in Chr04 are also discussed in Le Floc'h et al. (2003), giving either their observed R and absolute B -band magnitudes or their observed K magnitudes and colors, $R - K$. In addition to the Chr04 sample, we also consider two hosts for which the SFRs based on the rest-frame ultraviolet flux as well as the B -band magnitudes, are available. We can examine such hosts in a similar way as for the Chr04 sample. Masetti et al. (2005) discuss the properties of the host galaxy of GRB 000911 at

$z = 1.06$ and derive a B -band magnitude of around -18.4 , giving a $L_B/L_B^* = 0.09$ with our M_B^* (see section 2), and an extinction-corrected SFR_{UV} of $2.7 M_{\odot} \text{ yr}^{-1}$. Assuming an extincted SFR_{UV} to be a factor of 2 lower², gives a SFR-to-luminosity ratio around 15. The second host is that of GRB 030329 at $z = 0.168$. Gorosabel et al. (2005) derive a SFR_{UV} of $0.17 M_{\odot} \text{ yr}^{-1}$ and $M_B = -16.5$, giving a $SFR_{UV}/(L_B/L_B^*) = 10.6$. Note that this value is comparable to the SFR-to-luminosity ratios derived in the Chr04 sample. The counterparts of these two hosts are discussed near the end of this section.

3.2 Counterpart Identification

We generated catalogs of galaxies at the same redshifts as the observed hosts, and looked in each catalog for simulated galaxies that have both SFR_{UV} and $SFR_{UV}/(L_B/L_B^*)$ nearest to the corresponding values for each observed host. We are able to find a numerical counterpart to each of the 10 observed host of the Chr04 sample, although departures from the observationally inferred values may be large in some cases. The percentage errors in Table 1 quantify how close from these values the counterpart is found. They are defined by $\Delta X = |SFR_{UV}^{obs} - SFR_{UV}^{num}|/SFR_{UV}^{obs}$ and $\Delta Y = |\epsilon_L^{obs} - \epsilon_L^{num}|/\epsilon_L^{obs}$. In this last definition, ϵ_L denotes the SFR-to-luminosity ratio. The largest departures, when at least one of these quantities is larger than 5%, are seen for counterparts #3, 5 and 8. The first two are noted in Chr04 as having the least acceptable fits to their spectral energy distributions. The host of GRB 000418 (#3) is extensively discussed in Gorosabel et al. (2003) who analyze its spectral energy distribution using a variety of synthetic spectral templates. The adopted SFR does of course depend on the adopted SED. Also, Gorosabel et al. (2003) find the host galaxy of GRB 000210 (#5) to be brighter than the Chr04 estimate: They find that the B -band mag-

² The host of GRB 991208 has roughly similar B -band magnitude and A_V and has a ratio of un-extincted/extincted SFR within a factor of 2 (Chr04).

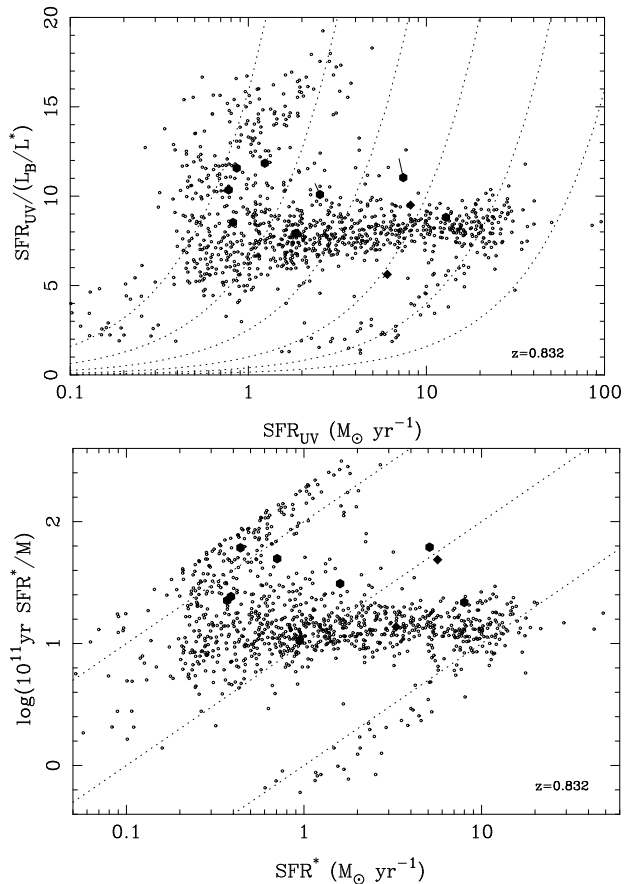


Figure 3. SFR-to-luminosity ratio versus SFR_{UV} (upper panel) and specific SFR versus SFR^* (lower panel) for the star-forming galaxy population at $z = 0.832$ (dots). The dotted curves in the upper panel denote constant M_B -values from -18 to -23 (left to right). In the lower panel the dotted lines indicate constant mass of 10^9 , 10^{10} and $10^{11} M_\odot$ (left to right). Although at different redshifts, the numerical counterparts of the observed host galaxies (listed in Table 1) are displayed in both panels (solid symbols): In decreasing order of SFR_{UV} , GRB 980703, 000926, 000418, 990123, 000210, 010921, 990712, 970508, 991208, 970228 (the order is the same in the bottom panel with SFR^* , except that the host of GRB 970228 is to the left of GRB 991208). In the upper panel, for each counterpart a short line segment indicates where the corresponding observed host galaxy would be found. In some cases the difference is too small for the line segment to be visible. The two diamonds denote the counterparts at the highest redshifts.

nitide is -20.16 , giving, with their $SFR_{UV} = 2.1 M_\odot \text{ yr}^{-1}$, a $SFR_{UV}/(L_B/L_B^*) = 4.5$ (10.7 in Chr04).³

Each numerical counterpart is characterized by a number of properties that are either tabulated in Table 1 or displayed in Fig. 3 and 5. The properties that are estimated directly from the simulation output are the star formation

³ Instead of adopting the nearest counterpart in each catalog, we could have looked for the second best closest counterparts or the counterparts within a given error box around each observed host. Because of the uncertainties in the observationally determined values and the small number of observed hosts in the sample we consider here, we do think that searching only for the closest counterpart is the most reasonable thing to do.

rate SFR^* , the specific SFR, the galaxy mass, the ratio $SFR^*/(SFR)$, the formation epoch of the first stellar population to form in the galaxy, and the epoch of formation of the galaxy as defined in section 2. From the computation of the SEDs we determine the star formation rate SFR_{UV} , the SFR-to-luminosity ratio, the magnitudes in the B and K -bands, the apparent R magnitude and the color, $R - K$. The mass-to-light ratios in the B and K -bands are then a combination of the primary simulation outputs and the observable properties.

3.3 'Observed' properties of the numerical counterparts

From Table 1 we note the following: Low-redshift hosts ($z < 0.9$) are low B -band luminosity galaxies, $M_B > -20$. We also see that the counterparts are fainter than -22 in the K -band at $z < 0.9$. The 10 counterparts are low-mass galaxies with $M < 4 \times 10^{10} M_\odot$ (the highest mass in the simulation at $z = 1$, being $7.4 \times 10^{11} M_\odot$). The B -band magnitudes and mass of the counterparts can also be seen in Fig. 3 discussed below, where in the upper panel the dotted curves denote values of constant $M_B = -18$ to -23 (from left to right) and in the lower panel the dashed lines indicate values of constant mass of 10^9 to $10^{11} M_\odot$ (from left to right). The counterparts have L_B/L_B^* between 0.074 and 1.46 and L_K/L_K^* between 0.028 and 0.84 (with $M_K^* = -24$), making most of them sub-luminous galaxies. The mass-to-light ratios in Table 1 are relatively small and more typical of late-type and dwarf galaxies than large spirals or elliptical galaxies.

The counterparts have apparent R -band magnitudes between 22 and 24.4 and comparison between those and the N-IR observational data reported in Le Floch et al. (2003) for the same hosts (here referred to as the common sample) shows that the candidate hosts #6 and #9 are the faintest and the brightest, respectively, both of our sample and of the common sample. The apparent R -band magnitudes of the counterparts are, however, generally slightly brighter than in Le Floch et al. (2003). The bluest of the 9 counterparts (#10) for which the $R - K$ colors of the corresponding hosts were estimated in Le Floch et al. (2003), is also the bluest of these 9 observed hosts. The observed host with the highest color index corresponds the counterpart with the second highest color index (after the least blue #2). Globally, we do find that 9 counterparts have $R - K$ colors between 2 and 2.9 and 3.5 for #2.

In Fig. 3 we superpose the numerical counterparts on a plot showing the simulated star-forming galaxy population at $z = 0.832$ in a diagram of SFR-to-luminosity ratio versus SFR_{UV} (upper panel) and in a diagram of specific SFR versus SFR^* (bottom panel). We have chosen $z = 0.832$ as it is roughly the median redshift of the sample. Rigorously speaking, only the counterpart of the host at $z = 0.832$ should be compared directly with the simulated catalog, since galaxy properties evolve with redshift. It may nevertheless be useful to plot the whole sample on a single diagram. We have used different symbols (diamonds) to mark the highest two redshifts, and will return to the issue of evolution later in this section. Each counterpart in the top panel is accompanied by a straight line, sometimes smaller than the symbol, that

indicates how well the properties of that numerical counterpart match those of the observed host (the difficulty in obtaining a good counterpart for host #3 is clearly seen). As noted above, the hosts have various SFRs, be it either the SFR_{UV} or the SFR^* , but they have high SFR-to-luminosity ratio and high specific rate, as they all lie in the upper half of both panels in Fig. 3. The specific SFR and the SFR-to-luminosity ratio would be even better correlated if the latter quantity is based on the K -band luminosity, according to the magnitude-mass diagrams in Fig. 2.

3.4 Comparison with the overall galaxy population

Even if some aspects of the simulation may be incomplete, it provides us with catalogs of galaxies at various redshifts in which different galaxy populations may be distinguished. After defining a particular sub-population of galaxies e.g. similar to the host galaxies of GRBs, an important issue is to compare this particular population to the overall galaxy population. Such a comparison is in the present case limited by the fact that the observed sample includes only 10 hosts, spanning a wide redshift range where cosmological evolution cannot be neglected.

3.4.1 The relationship between the specific SFR and the color index

We first conduct a qualitative comparison between the counterparts and the overall galaxy population at $z = 1$, focusing on the relationship between the specific SFR and the mass-to-light ratio and color index. By presenting observable properties at this redshift we follow-up on and extend the results and discussion of Paper I.

Figure 4 presents the mass-to-light ratios and color index of the whole galaxy population distinguished according to the specific rate ($\epsilon < 1$, $1 < \epsilon < 1.3$ and $\epsilon > 1.3$). We also plot the low-mass ($M < 5 \cdot 10^{10} M_\odot$) and high-mass ($M > 5 \cdot 10^{10} M_\odot$), non-star forming galaxies. We use the same threshold, $\epsilon = 1.3$, as in Paper I. It corresponds roughly to the peak of the probability density function of the specific SFR at $z = 1$. In addition, galaxies with specific rates below or above this value contribute about equally to the total star formation rate at that redshift. The top panel in Fig. 4 shows the large variation of the mass-to-light ratio with respect to the galaxy mass, but there is a clear correlation with the specific SFR (i.e. ϵ). High-mass non star-forming galaxies have large M/L_K , up to about 1, whereas the minimal value for the low-mass high-specific rate galaxies is ~ 0.15 . The mass-to-light ratio in the B -band, M/L_B , ranges between ~ 0.09 and ~ 3 , for the overall population. Recalling the results in Table 1, we note that the majority of the counterparts have $\log(M/L_K)$ between -0.5 and -0.3 , typical of our low-mass, high specific SFR galaxies, although it should be kept in mind that Fig. 4 is plotted at a single redshift ($z = 1$).

The color-magnitude diagram in the bottom panel in Fig. 4 shows a large variation of the color index $R - K$, from 1.5 up to 4.7, consistent with that seen in the recent K20 galaxy survey (Pozzetti et al. 2003). The high-mass, non star-forming galaxies, that are also old objects (see Paper I) have the highest color index, close to the typical value

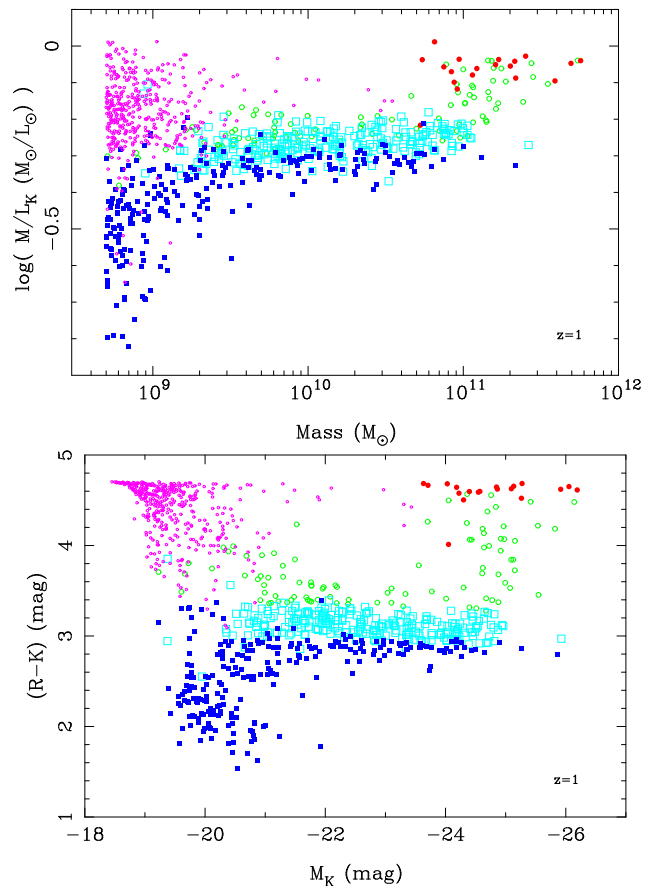


Figure 4. Mass-to-light ratio in solar units in the K -band as a function of mass (upper panel) and color-magnitude diagram (bottom panel) for the simulated galaxy population at $z = 1$. For clarity, only 1000 objects randomly selected from the catalog, are plotted. The dots indicate non star-forming, low-mass ($M < 5 \cdot 10^{10} M_\odot$) galaxies; the filled circles non star-forming, high-mass ($M > 5 \cdot 10^{10} M_\odot$) galaxies; the open circles star-forming galaxies with $\epsilon < 1$; the open squares star-forming galaxies with $1 < \epsilon < 1.3$; the filled squares star-forming galaxies with $\epsilon > 1.3$. Galaxies with a mass around $10^{11} M_\odot$, corresponding in Fig. 2 to the characteristic magnitude $M_{K_s}^* = -24.7$ (or $L_{K_s}^* = 1.6 \times 10^{11} L_\odot$), have a mass-to-light ratio of $\log(M/L_K) \sim -0.2$.

of old elliptical galaxies at $z \gtrsim 1$. In contrast, the majority of the star-forming galaxies have colors around 3. The color properties correlate with the specific SFR: The bluest objects are also faint galaxies with the highest specific rates. Comparing the data from Table 1 with Fig. 4 shows that the counterparts are clearly bluer than the high-mass star-forming galaxy population, with color index lower than ~ 3 . Recalling the correlation between mass and magnitude discussed in the previous section, we note that the colors and mass-to-light ratios are also tightly related (Bell & de Jong 2001). There is also a strong relation, albeit with some dispersion between mass and SFR, resulting in intermediate colors of the high-SFR galaxies. Therefore the blue and faint galaxies, typically characterized by high specific rates, are not the objects that have the highest SFRs.

Properties like the mass-to-light ratio and color index are generally considered to provide information on the star formation history of galaxies or how they assemble their

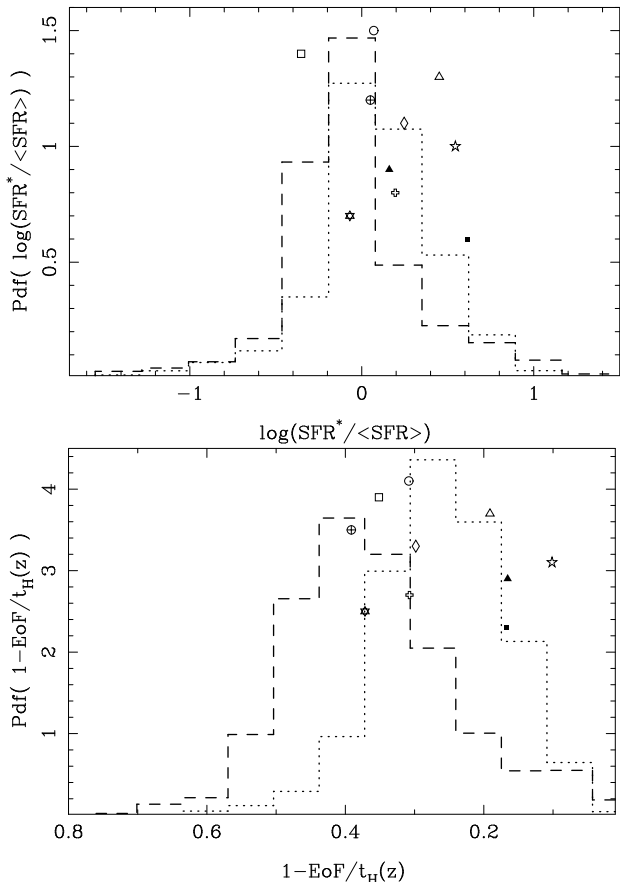


Figure 5. Probability density functions of the $SFR^*/\langle SFR \rangle$ (upper panel) and the epoch of formation EoF , when normalized to the Hubble time (bottom panel), for the star-forming galaxy populations at $z = 2.036$ (dotted) and $z = 0.832$ (dashed). The counterparts of the hosts in Table 1 are superposed at arbitrary ordinate, but in order of decreasing redshift (from top to bottom).

mass. They also tend to be more tightly correlated with the specific rate than the SFR. The $SFR^*/\langle SFR \rangle$, to be further discussed below, is another property that strongly correlates with the specific rate. As already pointed out in Paper I, but now confirmed using the calculated observable properties, we note the consistency between the observed properties of the GRB host galaxies: If host galaxies are blue and faint, they are expected not to be high-SFR and early-formed galaxies. The properties we have found for the counterparts confirm this conclusion.

3.4.2 The star-forming activity of the counterparts

Figure 5 compares the $SFR^*/\langle SFR \rangle$ and the epoch of formation of the counterparts to that of the star-forming galaxy population at $z = 0.832$ (dashed lines) and $z = 2.036$ (dotted lines), the highest redshift of the host sample. In each panel the counterparts are superposed on the distributions at arbitrary ordinate values, but with a decreasing redshift (from top to bottom). Strictly speaking only two hosts, #1 and #6, should be compared directly to their respective distributions.

The top panel compares the star-forming activity at a

given redshift of a galaxy to its average activity since the object started to form its stellar populations. Both distributions peak around unity, but the high-redshift distribution includes more galaxies with $SFR^*/\langle SFR \rangle > 1$, meaning that high-redshift galaxies are more active than present-day galaxies. All hosts except #2 have $SFR^*/\langle SFR \rangle$ close to or above unity (0.85 for #9).

The lower panel shows the epoch of formation normalized to the Hubble time. Comparing the distributions at the two redshifts shows that the low-redshift one is more extended but includes a non-negligible amount of objects with recent epochs of formation. All candidate hosts have ages within 40% of the age of the universe. We remind the reader that the distributions are constructed only from the star-forming galaxies and do not include the old, non star-forming galaxies. The epoch of formation indicates the epoch at which the galaxy was the most active and is expected to be quite different from the epoch of formation of the first stellar populations, t_{form} . Table 1 shows that the epoch of formation of the counterparts are indeed different from t_{form} . This particular time is relatively close to 1 (as defined in Table 1), meaning that the candidate hosts include an early-formed stellar population, although not dominant since they are at the same time young objects.

That the major fraction of the mass of most counterparts was assembled in the recent times is consistently shown by the specific rate, the ratio $SFR^*/\langle SFR \rangle$ and the epoch of formation. We note that the three hosts with the highest $SFR^*/\langle SFR \rangle$ ratios (counterparts #3, 6 and 10), also have the highest specific rates although their SFR^* and magnitudes differ widely (GRB 000418, 990712 and 970508, see Fig. 3). They are among the hosts with the youngest epochs of formation, the bluest $R-K$ colors, and the lowest mass-to-light ratios (Table 1), pointing again to the tight correlation between these galaxy properties as discussed above and to the consistency with the GRB host galaxy properties.

3.5 Discussion

Here, we emphasize our main result by comparing the SFR-to-luminosity ratios and specific SFRs of the numerical counterparts to the median values of these quantities in the catalogs they are selected from. These are displayed in Fig. 6. The median value of the specific SFR clearly increases with redshift. Note that at redshifts below $z \sim 0.7$, the minimal specific SFR tends to increase with decreasing redshift: This is due to the fact that the star formation of massive galaxies slows down as the redshift decreases and eventually ceases in an increasing number of them. They therefore disappear from the star-forming galaxy population. Comparing the specific SFRs and the SFR-to-luminosity ratio of the counterparts to the median values at similar redshift shows that the counterparts in all cases except one have values higher than the median. The only exception is the counterpart to GRB 990123 (#2). The $SFR_{UV}/(L_B/L_B^*)$ of this particular host is the lowest of the Chr04 sample and its observed spectral energy distribution was best fit by a star-forming Sa galaxy type, whereas all of the other hosts were fit by starburst templates. The B -band magnitude of this host could however be fainter (Bloom et al. 1999), giving a higher SFR-to-luminosity ratio. Moreover the $R-K$ color of this host is as blue as most of the hosts studied in

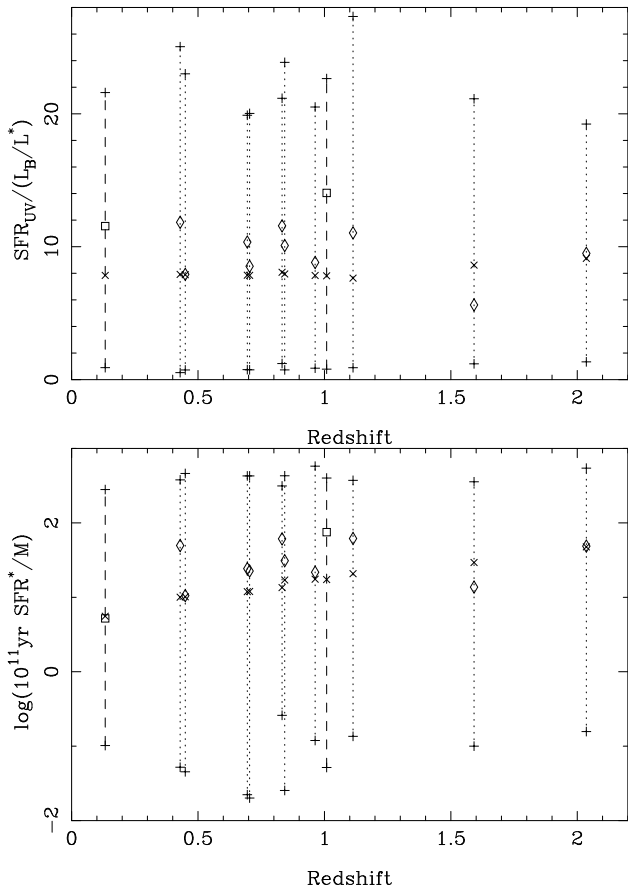


Figure 6. The median values (crosses) of the SFR-to-luminosity ratio (top) and specific SFR (bottom) for the star-forming galaxy populations at the redshifts of the GRB hosts. The range of values for each catalog is shown by the length of the vertical lines. Diamonds refer to the numerical counterpart in each case. The two squares are the counterparts of GRB 000911 and 030329 hosts that are briefly discussed at the end of Section 3.

Le Flocc’h et al. (2003), whereas it is the reddest one of our sample, as seen above (see Table 1).

It is interesting to note that Chary et al. (2002) estimate the specific SFRs of hosts #2, 4, 6, 7 and 8, although their observational study is based on extinction-corrected SFRs, and thus their derived specific rates are much higher than our results. The observed hosts #4, 6, 7, and 8 are among those with the highest specific SFR of the whole Chary et al. (2002) sample. They are also found to have higher specific rates than local starbursts have. The numerical counterparts to #6, 7 and 8 have specific rates well above the median values (the first three objects on the left in Fig. 3).

The two squares in Fig. 6 show the SFR-to-luminosity ratio and the specific SFR of the counterparts of the hosts of GRB 000911 and 030329, discussed at the beginning of this section. These counterparts were searched for in catalogs at slightly different redshifts from the host redshifts, $z = 1$ and $z = 0.133$, respectively. The counterpart of GRB 000911 ($\Delta X = 0.3\%$ and $\Delta Y = 5.2\%$) is a low-mass, young object ($M = 1.1 \times 10^9 M_\odot$, $1 - EoF/t_{H(z)} = 0.37$) with a high specific rate ($\epsilon = 1.87$), blue color $R - K = 2.12$ and a mass-to-light ratio $M/L_K = 0.36$. The closest counterpart that

we find for the host of GRB 030329 has a lower SFR-to-luminosity ratio than the observed estimate ($\Delta X = 1.7\%$ but $\Delta Y \sim 19\%$). The candidate host is a low-mass object ($M = 1.4 \times 10^9 M_\odot$), with blue color $R - K = 2.2$, a specific rate of $\epsilon = 0.7$ and an epoch of formation of $1 - EoF/t_{H(z)} = 0.45$. Compared to the overall population these two candidate hosts have SFR-to-luminosity ratios and specific SFRs well above or similar to the median values at the same redshifts.

The fact that the Chr04 sample is magnitude limited and includes bright hosts may explain why the numerical counterparts are not found among the objects with the highest possible specific SFRs. The counterpart of GRB 970508 (#6) is an example. From HST observations and other studies, this host may be described as a blue compact dwarf galaxy (Fruchter et al. 2000). Could this host be a prototype of the general host GRB galaxy population? Interestingly, the counterpart of this host could be found in the sample of compact galaxies at $z \sim 0.7$ analyzed in Guzman et al. (1997). The counterpart #6 ($z = 0.83$) with an absolute magnitude $M_B = -18.2$, a mass close to $10^9 M_\odot$ and a specific rate of $\epsilon \sim 1.8$ falls into the faintest and highest specific SFR population of compact galaxies in Guzman et al. (1997) (see their figures 5 and 7). Moreover, Sollerman et al. (2005) discuss three GRB host galaxies and show that they have similar properties as a sample of compact blue galaxies in the local universe.

4 CONCLUSIONS

In this paper, we have discussed cosmological galaxy properties and the properties of host galaxies of GRBs in particular, using fully hydrodynamic simulations of galaxy formation and the stellar population synthesis (SPS) code, *Starburst99*, to infer observable properties. An important feature of the numerical procedure is that the star formation history of galaxies entering the SPS code, comes directly from the simulation, with each stellar population contained in a given galaxy treated as a homogeneous population, that forms instantaneously. We identify objects in the simulation that have optical star formation rate, SFR_{UV} , and SFR-to-luminosity ratio, $SFR_{UV}/(L_B/L_\odot^*)$, similar to those estimated in a well-defined sample of ten observed host galaxies (Christensen et al. 2004), the only available homogeneous sample focusing on this ratio. Each numerical counterpart is selected from a simulated catalog at the same redshift as the corresponding observed host, and is characterized by a number of properties: The SFR^* , mass, specific SFR, $SFR^*/(SFR)$, epoch of formation of the first stellar population, and epoch of formation of the galaxy object. These are obtained directly from the simulation. In addition, B and K -band luminosities, R -band apparent magnitude, $R - K$ color, and mass-to-light ratios are obtained from the SPS or combination of both results. It should be emphasized that some of these properties (e.g. mass and SFR^*) are estimated directly from the simulations, making their definition inherently different from those commonly adopted in observations.

The Christensen et al. (2004) sample includes host galaxies with redshifts in the range $0.43 < z < 2.03$. The sample is magnitude-limited ($R < 25.3$), with estimated ab-

solute B -band magnitudes between -21.4 and -18.1 . Our counterpart hosts are low-mass galaxies ($M < 4 \cdot 10^{10} M_{\odot}$), with low mass-to-light ratios (M/L_B around 0.5); most of them are blue ($R-K < 2.9$) and young galaxies, with epochs of formation (or ages), within 40% of the age of the universe at the different redshifts. Although the SFR^* of the counterparts varies between ~ 0.4 and $8 M_{\odot} \text{ yr}^{-1}$, the specific SFR is equal to or higher than the median values estimated for the different catalogs, with the lowest value being $\epsilon \sim 1$. Because of its strong correlation with the specific rate, the $SFR^*/\langle SFR \rangle$ also has high values, around unity or higher. To outline the consistency of such an ensemble of properties, we compare the counterparts to the overall galaxy population at intermediate redshift and discuss the strong relationships between the specific SFR and quantities known to reflect the star formation history of galaxies, i.e. color and mass-to-light ratio. Indeed, the bluest objects are also faint galaxies with the highest specific rates.

Our identification of simulated galaxies with observed hosts has some limitations, both from observational and numerical points of view. Some of the observed hosts may, in other observational studies, be found to have slightly different SFRs or magnitudes, making their SFR-to-luminosity ratios uncertain. Although the general agreement between the simulation and the observations is fairly good, it should be kept in mind that the moderate resolution and somewhat limited number of physical processes included in the simulation may affect the relative number of galaxies in each sub-population. For instance, these simulations only account for a limited number of “extreme”-type galaxies, such as extreme starbursts or massive star-forming galaxies. Furthermore, we do not include the effects of dust and, as in Christensen et al. (2004), we only consider extincted SFR_{UV} in the estimate of the $SFR_{UV}/(L_B/L_B^*)$ ratio. That may not be a serious drawback since our focus is on low-mass galaxies that on average suffer less attenuation than the massive ones. In addition, the amount of dust has been shown to be limited in most host galaxies of GRBs (Le Floc’h et al. 2006). The main limitation of this study is the wide redshift range of the 10 observed host galaxies, with only a few galaxies in each narrow redshift bin. The inferences made therefrom need to be confirmed once the sample size has grown by a factor of 5-10, with a number of hosts at similar redshifts. We should expect to see still higher specific rates in low-mass objects, as the simulated catalogs tend to show. The evolutionary effects displayed in Fig. 6 support this conclusion.

Comparing an expanded host galaxy sample based on Swift data with the simulated catalogs and other well-known galaxy sub-populations, such as compact blue galaxies may be extremely useful. Hosts galaxies should provide a clearer view into the formation and evolution of galaxies and the role of different sub-populations therein. In particular, they will help in investigating the faint end of the galaxy luminosity function. Our results, obtained using a numerical approach, are consistent with and confirm the picture of GRB host galaxies that has emerged lately: They tend to have low mass, be blue in color and have relatively high specific star formation rates. Host galaxies may then belong to the high specific SFR galaxy population, rather than the high SFR population. High-resolution simulations are required to determine, in a more quantitative way, the contribution of the

host galaxies to the overall population, and whether hosts are a part of the average normal star-forming galaxy population or a sub-population of this one, with blue and very low-luminosity objects.

ACKNOWLEDGMENTS

We thank Jens Hjorth and Johan Fynbo for many interesting discussion sessions on GRB galaxy hosts and their properties. We also thank the anonymous referee for comments that helped us improve the presentation. This research was supported in part by a special grant from the Icelandic Research Council. The numerical simulations used in this paper were performed on NEC-SX6 of the High Performance Computing Center Stuttgart (HLRS) of the University of Stuttgart (Germany).

REFERENCES

- Bell E. F., de Jong R. S., 2001, *ApJ*, 550, 212
 Bell E. F., Papovich C., Wolf C., Le Floc’h E., Caldwell J. A. R., Barden M., Egami E., McIntosh D. H., Meisenheimer K., Pérez-González P. G., Rieke G. H., Rieke M. J., Rigby J. R., Rix H.-W., 2005, *ApJ*, 625, 23
 Berger E., Penprase B. E., Cenko S. B., Kulkarni S. R., Fox D. B., Steidel C. C., Reddy N. A., 2005, arXiv:astro-ph/0511498
 Berger E., Penprase B. E., Fox D. B., Kulkarni S. R., Hill G., Schaefer B., Reed M., 2005, arXiv:astro-ph/0512280
 Bicker J., Fritze-v. Alvensleben U., 2005, *A&A*, 443, L19
 Bloom J. S., Odewahn S. C., Djorgovski S. G., Kulkarni S. R., Harrison F. A., Koresko C., Neugebauer G., Armus L. e. a., 1999, *ApJL*, 518, L1
 Boselli A., Gavazzi G., Donas J., Scodreggio M., 2001, *AJ*, 121, 753
 Brinchmann J., Charlot S., White S. D. M., Tremonti C., Kauffmann G., Heckman T., Brinkmann J., 2004, *MNRAS*, 351, 1151
 Bruzual G., Charlot S., 2003, *MNRAS*, 344, 1000
 Cervino M., Luridiana V., 2005, arXiv:astro-ph/0510411
 Chary R., Becklin E. E., Armus L., 2002, *ApJ*, 566, 229
 Christensen L., Hjorth J., Gorosabel J., 2004, *A&A*, 425, 913 (Chr04)
 Cole S., Norberg P., Baugh C. M., Frenk C. S., Bland-Hawthorn J., Bridges T., Cannon R., Colless M. e. a., 2001, *MNRAS*, 326, 255
 Courty S., Björnsson G., Gudmundsson E. H., 2004, *MNRAS*, 354, 581 (Paper I)
 Feulner G., Gabasch A., Salvato M., Drory N., Hopp U., Bender R., 2005, *ApJL*, 633, L9
 Fruchter A. S., Pian E., Gibbons R., Thorsett S. E., Ferguson H., Petro L., Sahu K. C., Livio M. e. a., 2000, *ApJ*, 545, 664
 Fruchter A. S., Thorsett S. E., Metzger M. R., Sahu K. C., Petro L., Livio M., Ferguson H., Pian E. e. a., 1999, *ApJL*, 519, L13
 Fynbo J. P. U., Jakobsson P., Möller P., Hjorth J., Thomsen B., Andersen M. I., Fruchter A. S., Gorosabel J. e. a., 2003, *A&A*, 406, L63

- Gorosabel J., Christensen L., Hjorth J., Fynbo J. U., Pedersen H., Jensen B. L., Andersen M. I., Lund N. e. a., 2003, *A&A*, 400, 127
- Gorosabel J., Klose S., Christensen L., Fynbo J. P. U., Hjorth J., Greiner J., Tanvir N., Jensen B. L. e. a., 2003, *A&A*, 409, 123
- Gorosabel J., Pérez-Ramírez D., Sollerman J., de Ugarte Postigo A., Fynbo J. P. U., Castro-Tirado A. J., Jakobsen P., Christensen L. e. a., 2005, *A&A*, 444, 711
- Grazian A., Fernandez-Soto A., Testa V., Fugazza D., D'Avanzo P., 2006, *GRB Coordinates Network*, 4545, 1
- Guzman R., Gallego J., Koo D. C., Phillips A. C., Lowenthal J. D., Faber S. M., Illingworth G. D., Vogt N. P., 1997, *ApJ*, 489, 559
- Hjorth J., Sollerman J., Møller P., Fynbo J. P. U., Woosley S. E., Kouveliotou C., Tanvir N. R., Greiner J. e. a., 2003, *Nature*, 423, 847
- Jakobsson P., et al. 2006, *A&A*, 447, 897
- Jaunsen A. O., Andersen M. I., Hjorth J., Fynbo J. P. U., Holland S. T., Thomsen B., Gorosabel J., Schaefer B. E., Björnsson G., Natarajan P., Tanvir N. R., 2003, *A&A*, 402, 125
- Kawai N., Yamada T., Kosugi G., Hattori T., Aoki K., 2005, *GRB Coordinates Network*, 3937, 1
- Kennicutt R. C., 1998, *ARAA*, 36, 189
- Kennicutt R. C., Tamblyn P., Congdon C. E., 1994, *ApJ*, 435, 22
- Le Flo'c'h E., Charmandaris V., Forrest W. J., Mirabel I. F., Armus L., Devost D., 2006, *ApJ*, 642, 636
- Le Flo'c'h E., Duc P.-A., Mirabel I. F., Sanders D. B., Bosch G., Diaz R. J., Donzelli C. J., Rodrigues I., Courvoisier T. J.-L., Greiner J., Mereghetti S., Melnick J., Maza J., Minniti D., 2003, *A&A*, 400, 499
- Leitherer C., Schaerer D., Goldader J. D., Delgado R. M. G., Robert C., Kune D. F., de Mello D. F., Devost D., Heckman T. M., 1999, *ApJS*, 123, 3
- Masetti N., Palazzi E., Pian E., Hunt L., Fynbo J. P. U., Gorosabel J., Klose S., Benetti S. e. a., 2005, *A&A*, 438, 841
- Piran T., 2005, *Reviews of Modern Physics*, 76, 1143
- Pozzetti L., Cimatti A., Zamorani G., Daddi E., Menci N., Fontana A., Renzini A., Mignoli M., Poli F., Saracco P., Broadhurst T., Cristiani S., D'Odorico S., Giallongo E., Gilmozzi R., 2003, *A&A*, 402, 837
- Smith I. A., Tilanus R. P. J., Tanvir N., Barnard V. E., Moriarty-Schieven G. H., Frail D. A., Wijers R. A. M. J., Vreeswijk P. e. a., 2005, *A&A*, 439, 987
- Sokolov V. V., Fatkhullin T. A., Castro-Tirado A. J., Fruchter A. S., Komarova V. N., Kasimova E. R., Dodonov S. N., Afanasiev V. L. e. a., 2001, *A&A*, 372, 438
- Sollerman J., Östlin G., Fynbo J. P. U., Hjorth J., Fruchter A., Pedersen K., 2005, *New Astronomy*, 11, 103
- Stanek K. Z., Matheson T., Garnavich P. M., Martini P., Berlind P., Caldwell N., Challis P., Brown W. R., Schild R. e. a., 2003, *ApJL*, 591, L17
- Sullivan M., Mobasher B., Chan B., Cram L., Ellis R., Treyer M., Hopkins A., 2001, *ApJ*, 558, 72
- Tagliaferri G., Antonelli L. A., Chincarini G., Fernández-Soto A., Malesani D., Della Valle M., D'Avanzo P., Grazian A., Testa V., Campana S., Castro-Tirado A. J., Romano P., 2005, *A&A*, 443, L1
- Totani T. e., 2005, *ArXiv Astrophysics e-prints*
- Vázquez G. A., Leitherer C., Heckman T. M., 2005, *ApJ*, 621, 695